European Congress on Computational Methods in Applied Sciences and Engineering
ECCOMAS 2004
P. Neittaanmäki, T. Rossi, S. Korotov, E. Oñate, J. Périaux, and D. Knörzer (eds.)
Jyväskylä, 24–28 July 2004

MULTIDIMENSIONAL FEM-TVD PARADIGM FOR CONVECTION-DOMINATED FLOWS

Dmitri Kuzmin* **and Stefan Turek**

Institute of Applied Mathematics (LS III), University of Dortmund
Vogelpothsweg 87, D-44227, Dortmund, Germany
*e-mail: kuzmin@math.uni-dortmund.de, web page: http://www.mit.jyu.fi/kuzmin

Key words: Convection-Dominated Flows, Navier-Stokes Equations, $k-\varepsilon$ Turbulence Model, High-Resolution Schemes, Finite Elements, Unstructured Meshes

Abstract. *An algebraic approach to the design of multidimensional high-resolution schemes is introduced and elucidated in the finite element context. A centered space discretization of unstable convective terms is rendered local extremum diminishing by a conservative elimination of negative off-diagonal coefficients from the discrete transport operator. This modification leads to an upwind-biased low-order scheme which is nonoscillatory but overly diffusive. In order to reduce the incurred error, a limited amount of compensating antidiffusion is added in regions where the solution is sufficiently smooth. A node-oriented flux limiter of TVD type is designed so as to control the ratio of upstream and downstream edge contibutions to each node. Nonlinear algebraic systems are solved by an iterative defect correction scheme preconditioned by the low-order evolution operator which enjoys the M-matrix property. The diffusive and antidiffusive terms are represented as a sum of antisymmetric internodal fluxes which are constructed edge-by-edge and inserted into the global vectors. The new methodology is applied to the equations of the $k-\varepsilon$ turbulence model and relevant implementation aspects are addressed. Numerical results are presented for the three-dimensional incompressible flow over a backward facing step.*

1 INTRODUCTION

The class of *total variation diminishing* (TVD) methods was introduced by Harten [6] two decades ago and carried over to unstructured grid finite element methods in [10],[11]. A node-oriented flux limiter of TVD type was designed so as to render an oscillatory high-order discretization local extremum diminishing (LED) via conservative matrix manipulations. This straightforward 'postprocessing' technique is applicable to discrete operators of any origin regardless of the underlying mesh and of the time-stepping scheme. Moreover, it is readily portable to multidimensions and can be integrated into existing CFD codes as a modular extension to the matrix assembly routine. In the present paper, we apply the FEM-TVD algorithm to incompressible flow problems and dwell on the implementation of the $k-\varepsilon$ turbulence model. Three-dimensional numerical examples illustrate the performance of the proposed simulation tools. An extension of the *algebraic flux correction* paradigm to the Euler equations of gas dynamics is presented in [11].

2 ALGEBRAIC CONSTRAINTS

First of all, let us introduce the algebraic constraints which should be imposed on the discrete operators to prevent the formation of spurious undershoots and overshoots in the vicinity of steep gradients. As a model problem, consider the continuity equation

$$\frac{\partial u}{\partial t}+\nabla\cdot(\mathbf{v}u)=0 \tag{1}$$

discretized in space by a numerical method which yields an ODE system of the form

$$\frac{\mathrm{d}u_i}{\mathrm{d}t}=\sum_{j\neq i}c_{ij}(u_j-u_i),\qquad \forall i. \tag{2}$$

It was shown by Jameson [7] that if the coefficients c_{ij} are nonnegative, then the semi-discrete scheme is *local extremum diminishing* (LED). Indeed, if a maximum is attained at node i, then each term in the sum over $j\neq i$ is less than or equal to zero and so is the time derivative of the nodal value u_i. So a maximum cannot increase, and in much the same way one can show that a minimum cannot decrease. For three-point finite difference methods, this requirement reduces to Harten's TVD conditions. Therefore, LED schemes are total variation diminishing in the 1D case. At the same time, Jameson's criterion is more general and turns out to be very handy in multidimensions, since the sign of matrix entries is easy to verify for arbitrary discretizations on unstructured meshes.

After the time discretization, an additional constraint should be imposed to make sure that quantities like densities, temperatures or concentrations remain nonnegative. In general, a fully discrete scheme is *positivity-preserving* if it admits the representation

$$Au^{n+1}=Bu^n, \tag{3}$$

where $B=\{b_{ij}\}$ has no negative entries and $A=\{a_{ij}\}$ is a so-called *M-matrix* defined as a nonsingular discrete operator such that $a_{ij}\leq 0$ for $j\neq i$ and all the coefficients of its

inverse are nonnegative. These properties imply that the positivity of the old solution u^n carries over to $u^{n+1} = A^{-1}Bu^n$. As a useful byproduct, this algebraic criterion yields a readily computable upper bound for admissible time steps. In particular, LED schemes of the form (2) are unconditionally positivity-preserving for $\theta = 1$ (backward Euler method) and subject to the following CFL-like condition otherwise [9]

$$\max_i |c_{ii}^n| \, \Delta t \leq \frac{1}{1-\theta}, \qquad \text{for} \quad 0 \leq \theta < 1. \tag{4}$$

Note that this estimate is based solely on the magnitude of the diagonal coefficients c_{ii}^n.

3 DESIGN OF HIGH-RESOLUTION SCHEMES

The basic idea for the derivation of an algebraic high-resolution scheme is rather simple. It can be traced back to the concepts of flux-corrected transport introduced by Boris and Book in the early 1970s [1]. Roughly speaking, the governing equation is discretized in space by an arbitrary linear high-order method (e.g. central differences or Galerkin FEM) and the resulting matrices are modified *a posteriori* so as to enforce the above algebraic constraints at the (semi-)discrete level. The flow chart of required algebraic manipulations is sketched in Fig. 1. The time step Δt should be chosen so as to satisfy condition (4).

1. Linear high-order scheme (e.g. Galerkin FEM)

$$M_C \frac{\mathrm{d}u}{\mathrm{d}t} = Ku \quad \text{such that} \quad \exists\, j \neq i:\ k_{ij} < 0$$

2. Linear low-order scheme $L = K + D$

$$M_L \frac{\mathrm{d}u}{\mathrm{d}t} = Lu \quad \text{such that} \quad l_{ij} \geq 0,\ \forall j \neq i$$

3. Nonlinear high-resolution scheme $K^* = L + F$

$$M_L \frac{\mathrm{d}u}{\mathrm{d}t} = K^*u \quad \text{such that} \quad \exists\, j \neq i:\ k_{ij}^* < 0$$

Equivalent representation $L^*u = K^*u$ is LED

$$M_L \frac{\mathrm{d}u}{\mathrm{d}t} = L^*u \quad \text{such that} \quad l_{ij}^* \geq 0,\ \forall j \neq i$$

Figure 1: Roadmap of matrix manipulations.

First, the consistent mass matrix M_C is replaced by its lumped counterpart M_L and the high-order operator K is transformed into a nonoscillatory low-order one by adding a discrete diffusion operator D designed so as to get rid of all negative off-diagonal coefficients. In accordance with the well-known Godunov theorem, this manipulation results in a global loss of accuracy. In order to prevent excessive smearing in smooth regions, it is necessary to remove as much artificial diffusion as possible without generating wiggles. To this end, a limited amount of compensating antidiffusion F is added in the next step. Even though the final transport operator K^* does have negative off-diagonal coefficients, they are harmless as long as there exists an equivalent LED representation of the modified scheme. For a given solution vector u, there should exist a matrix L^* such that all off-diagonal entries l_{ij}^* are nonnegative and $L^*u = K^*u$. Following these guidelines, let us derive the operators D and F for a multidimensional FEM-TVD algorithm.

4 DISCRETE UPWINDING

Let us perform mass lumping in the left-hand side of the Galerkin scheme and represent the semi-discretized equation for the nodal value u_i as follows

$$m_i \frac{\mathrm{d}u_i}{\mathrm{d}t} = \sum_{j \neq i} k_{ij}(u_j - u_i) + \delta_i u_i, \qquad \delta_i = \sum_j k_{ij}. \tag{5}$$

The elimination of negative off-diagonal coefficients does not affect the term $\delta_i u_i$ which vanishes for divergence-free velocity fields and is responsible for a physical growth of local extrema otherwise [11]. The artificial diffusion operator D is designed to be a symmetric matrix with zero row and column sums. Therefore, the diffusive term Du can be decomposed into a sum of antisymmetric numerical fluxes between neighboring nodes

$$(Du)_i = \sum_{j \neq i} f_{ij}^d, \qquad \text{where} \quad f_{ij}^d = d_{ij}(u_j - u_i), \quad f_{ji}^d = -f_{ij}^d. \tag{6}$$

In practice, we start with the high-order operator $L := K$ and examine each pair of nonzero off-diagonal coefficients k_{ij} and k_{ji} which corresponds to an edge $\overrightarrow{ij}$ of the sparsity graph. The 'optimal' artificial diffusion coefficient d_{ij} is given by [8],[9]

$$d_{ij} = \max\{0, -k_{ij}, -k_{ji}\}. \tag{7}$$

If the smaller off-diagonal coefficient, say k_{ij}, is negative, then $l_{ij} = k_{ij} + d_{ij}$ is equal to zero and three other entries are modified so as to restore the row/column sums

$$\begin{aligned} l_{ii} &:= l_{ii} - d_{ij}, \qquad & l_{ij} &:= l_{ij} + d_{ij}, \\ l_{ji} &:= l_{ji} + d_{ij}, \qquad & l_{jj} &:= l_{jj} - d_{ij}. \end{aligned} \tag{8}$$

The edge is oriented so that $l_{ji} \geq l_{ij} = \max\{0, k_{ij}\}$. This convention implies that node i is located 'upwind', which enables us to derive an upwind-biased scheme of TVD type.

5 ALGEBRAIC FLUX CORRECTION OF TVD TYPE

The elimination of negative off-diagonal matrix entries corresponds to the upwind difference approximation in the 1D case [9],[11]. This is why it is called 'discrete upwinding'. By construction, the resulting scheme is the least diffusive linear LED counterpart of the original Galerkin discretization. Nevertheless, its accuracy leaves a lot to be desired and should be enhanced by adding a **nonlinear** antidiffusive correction to the low-order operator. The task of the flux limiter is to make sure that the final transport operator $K^* = L + F = K + D + F$ admits an equivalent LED representation (see Fig. 1).

In practice, the antidiffusive term Fu is assembled edge-by-edge as follows

$$(Fu)_i = \sum_{j \neq i} f_{ij}^a \qquad \text{such that} \quad f_{ji}^a = -f_{ij}^a, \tag{9}$$

where the limited antidiffusive flux f_{ij}^a from node j into its upwind (in the sense of our orientation convention) neighbor i depends on the diffusion coefficient d_{ij} for discrete upwinding and on the entry $l_{ji} = \max\{k_{ji}, k_{ji} - k_{ij}\}$ of the low-order transport operator

$$f_{ij}^a := \min\{\Phi(r_i) d_{ij}, l_{ji}\}(u_i - u_j). \tag{10}$$

Here Φ is a standard TVD limiter (e.g. *minmod*, Van Leer, MC, *superbee*) applied to a suitable smoothness indicator r_i (to be specified below). At the same time, the antidiffusive flux into node j is defined as $f_{ji}^a := -f_{ij}^a$ so that mass conservation is guaranteed.

Let us derive a sufficient condition for the modified scheme to be local extremum diminishing. If $\Phi(r_i) = 0$ or $d_{ij} = 0$, the antidiffusive flux f_{ij}^a vanishes and does not pose any hazard. Therefore, we restrict ourselves to the nontrivial case $f_{ij}^a \neq 0$ which implies that both $\Phi(r_i)$ and d_{ij} are strictly positive. The symmetry property of TVD limiters [7] makes it possible to represent the antidiffusive flux in the form

$$f_{ij}^a = \Phi(r_i) a_{ij}(u_i - u_j) = \Phi(1/r_i) a_{ij} \Delta u_{ij}, \tag{11}$$

where the *antidiffusion coefficient* a_{ij} and the *upwind difference* Δu_{ij} are defined as follows

$$a_{ij} := \min\{d_{ij}, l_{ji}/\Phi(r_i)\}, \qquad \Delta u_{ij} := r_i(u_i - u_j). \tag{12}$$

The assumption $d_{ij} > 0$ implies that $k_{ij} < 0$ and $l_{ij} = 0$ for the edge $\overrightarrow{ij}$ which links an upwind node i and a downwind node j. Therefore, the edge contributions to the two components of the modified convective term K^*u can be written as

$$k_{ij}^*(u_j - u_i) = f_{ij}^a, \qquad k_{ji}^*(u_i - u_j) = l_{ji}(u_i - u_j) - f_{ij}^a. \tag{13}$$

The increment to node j is obviously of diffusive nature and satisfies the LED criterion, since the coefficient $k_{ji}^* = l_{ji} - \Phi(r_i) a_{ij}$ is nonnegative by construction (see the definition of a_{ij}). Furthermore, it follows from relation (11) that the negative off-diagonal entry

$k_{ij}^* = -\Phi(r_i)a_{ij}$ of the nonlinear operator K^* is acceptable provided that the auxiliary quantity Δu_{ij} admits the following representation

$$\Delta u_{ij} = \sum_{k\neq i} \sigma_{ik}(u_k - u_i), \qquad \text{where} \quad \sigma_{ik} \geq 0, \quad \forall k \neq i. \tag{14}$$

In other words, the limited antidiffusive flux f_{ij}^a from node j into node i should be interpreted as a sum of diffusive fluxes contributed by other neighbors.

5.1 NODE-ORIENTED FLUX LIMITER

Let us introduce a fully multidimensional limiting strategy which is akin to that proposed by Zalesak [20] in the framework of flux-corrected transport (FCT) methods. The incompressible part of the original convective term Ku can be decomposed into a sum of edge contributions with negative coefficients and a sum of those with positive coefficients

$$P_i = \sum_{j\neq i} \min\{0, k_{ij}\}(u_j - u_i), \qquad Q_i = \sum_{j\neq i} \max\{0, k_{ij}\}(u_j - u_i) \tag{15}$$

which are due to mass transfer from the downstream and upstream directions, respectively. The sum P_i is composed from the *raw antidiffusive fluxes* which offset the error incurred by elimination of negative matrix entries in the course of discrete upwinding. They are responsible for the formation of spurious wiggles and must be securely limited. At the same time, the constituents of the sum Q_i are harmless since they resemble diffusive fluxes and do satisfy the LED criterion. Thus, it is natural to require that the net antidiffusive flux into node i be a limited average of the original increments P_i and Q_i. Furthermore, it is worthwhile to distinguish between the positive and negative edge contributions

$$P_i = P_i^+ + P_i^-, \qquad P_i^\pm = \sum_{j\neq i} \min\{0, k_{ij}\} \underset{\max}{\min} \{0, u_j - u_i\}, \tag{16}$$

$$Q_i = Q_i^+ + Q_i^-, \qquad Q_i^\pm = \sum_{j\neq i} \max\{0, k_{ij}\} \underset{\min}{\max} \{0, u_j - u_i\} \tag{17}$$

and limit the positive and negative antidiffusive fluxes separately. To this end, we pick a standard TVD limiter Φ and compute the *nodal correction factors*

$$R_i^\pm = \Phi(Q_i^\pm / P_i^\pm) \tag{18}$$

which determine the percentage of $P_i^\pm$ that can be retained without violating the LED constraint for row i of the modified transport operator K^*.

For each edge $\overrightarrow{ij}$ of the sparsity graph, the antidiffusive flux f_{ij}^a from its downwind node j into the upwind node i is constructed as follows [10]

$$f_{ij}^a := \begin{cases} \min\{R_i^+ d_{ij}, l_{ji}\}(u_i - u_j) & \text{if } u_i \geq u_j, \\ \min\{R_i^- d_{ij}, l_{ji}\}(u_i - u_j) & \text{if } u_i < u_j, \end{cases} \qquad f_{ji}^a := -f_{ij}^a. \tag{19}$$

Importantly, the same correction factor $R_i^{\pm}$ is applied to all positive/negative antidiffusive fluxes which represent the interactions of node i with its neighbors located downstream.

The node-oriented limiting strategy makes it possible to control the combined effect of antidiffusive fluxes *acting in concert* and prove the LED property. The equivalence of (10) and (19) reveals that the smoothness indicator r_i is implicitly defined by

$$r_i = \begin{cases} Q_i^+/P_i^+ & \text{if } \ u_i \geq u_j, \\ Q_i^-/P_i^- & \text{if } \ u_i < u_j. \end{cases} \tag{20}$$

It is easy to verify that $\Delta u_{ij} = r_i(u_i - u_j)$ satisfies condition (14) since all coefficients in the sum of upwind contributions $Q_i^{\pm}$ are nonnegative and

$$\Delta u_{ij} = \sigma_{ij} Q_i^{\pm}, \qquad \text{where} \quad \sigma_{ij} = \min_{\max} \{0, u_i - u_j\}/P_i^{\pm} \geq 0. \tag{21}$$

Remarkably, the new limiter extracts all information from the original matrix K and does not need the coordinates of nodes or other geometric details. For the one-dimensional convection equation with a constant velocity, a classical TVD scheme is recovered [10].

6 ITERATIVE DEFECT CORRECTION

After an implicit time discretization, one obtains a nonlinear algebraic system

$$M_L \frac{u^{n+1} - u^n}{\Delta t} = \theta K^*(u^{n+1})u^{n+1} + (1-\theta)K^*(u^n)u^n, \qquad 0 < \theta \leq 1$$

which can be solved iteratively by the fixed-point defect correction scheme [10]

$$u^{(m+1)} = u^{(m)} + A^{-1} r^{(m)}, \qquad m = 0, 1, 2, \ldots \tag{22}$$

where $r^{(m)}$ denotes the residual for the m-th cycle and A is a suitably chosen 'preconditioner' which should be easy to 'invert' by solving the linear subproblem

$$A \Delta u^{(m+1)} = r^{(m)}, \qquad m = 0, 1, 2, \ldots \tag{23}$$

and applying the resulting solution increment $\Delta u^{(m+1)}$ to the last iterate

$$u^{(m+1)} = u^{(m)} + \Delta u^{(m+1)}, \qquad u^{(0)} = u^n. \tag{24}$$

The low-order evolution operator $A = M_L - \theta \Delta t L$ constructed by resorting to discrete upwinding ($L = K + D$) constitutes an excellent preconditioner for it was designed to be an M-matrix. The defect vector and the constant right-hand side are given by

$$r^{(m)} = b^n - [A - \theta \Delta t F(u^{(m)})]u^{(m)}, \quad b^n = M_L u^n + (1-\theta)\Delta t [L + F(u^n)]u^n. \tag{25}$$

Both expressions consist of a low-order contribution augmented by the sum of limited antidiffusive fluxes which are evaluated edge-by-edge and inserted into the global vectors.

7 FEM-TVD FOR THE $k-\varepsilon$ MODEL

High-resolution schemes like FEM-TVD play an increasingly important role in the numerical simulation of turbulent flows. The flow structures that cannot be resolved on the computational mesh activate the flux limiter which curtails the raw antidiffusion so as to filter out the small-scale fluctuations. Interestingly enough, the residual artificial viscosity provides an excellent subgrid scale model for the Monotonically Integrated Large Eddy Simulation (MILES) [2]. RANS turbulence models constitute a cost-effective alternative to this approach and also call for the use of a positivity-preserving discretization.

In particular, the evolution of the turbulent kinetic energy k and of its dissipation rate ε is governed by two convection-dominated transport equations

$$\frac{\partial k}{\partial t} + \nabla \cdot \left(k\mathbf{u} - \frac{\nu_T}{\sigma_k} \nabla k \right) = P_k - \varepsilon, \tag{26}$$

$$\frac{\partial \varepsilon}{\partial t} + \nabla \cdot \left(\varepsilon\mathbf{u} - \frac{\nu_T}{\sigma_\varepsilon} \nabla \varepsilon \right) = \frac{\varepsilon}{k}(C_1 P_k - C_2 \varepsilon), \tag{27}$$

where $\mathbf{u}$ denotes the averaged velocity, $\nu_T = C_\mu k^2/\varepsilon$ is the turbulent eddy viscosity and $P_k = \frac{\nu_T}{2}|\nabla\mathbf{u} + \nabla\mathbf{u}^T|^2$ is the production term. For the standard $k-\varepsilon$ model, we have

$$C_\mu = 0.09, \quad C_1 = 1.44, \quad C_2 = 1.92, \quad \sigma_k = 1.0, \quad \sigma_\varepsilon = 1.3.$$

Note that the transport equations for k and ε are strongly coupled and nonlinear so that their numerical solution is anything but trivial. Implementation details and employed 'tricks' are rarely reported in the literature, so that a novice to this area of CFD research often needs to reinvent the wheel. Thus, we deem it appropriate to discuss the implementation of a FEM-TVD algorithm for the $k-\varepsilon$ model in some detail. The concomitant incompressible Navier-Stokes equations are solved by a discrete projection method from the family of Multilevel Pressure Schur Complement (MPSC) schemes [19] implemented in the open-source software package FEATFLOW (see *http://www.featflow.de*).

7.1 Positivity-preserving linearization

The block-iterative algorithm proposed in [12] consists of nested loops so that the coupled PDE system is replaced by a sequence of linear subproblems. The coefficients are 'frozen' during each outer iteration and updated as new solution values become available. The quasi-linear transport equations can be solved by an implicit FEM-TVD scheme but the linearization procedure must be tailored to the need to preserve the positivity of k and ε in a numerical simulation. Due to the presence of sink terms in the right-hand side of both equations, the positivity constraint may be violated even if a high-resolution scheme is employed for the discretization of convective terms. It can be proved that the exact solution to the $k-\varepsilon$ model remains nonnegative for positive initial data [16],[17] and it is essential to guarantee that the numerical scheme will also possess this property.

Let us consider the following representation of the equations at hand [14]

$$\frac{\partial k}{\partial t} + \nabla \cdot (k\mathbf{u} - d_k \nabla k) + \gamma k = P_k, \tag{28}$$

$$\frac{\partial \varepsilon}{\partial t} + \nabla \cdot (\varepsilon \mathbf{u} - d_\varepsilon \nabla \varepsilon) + C_2 \gamma \varepsilon = C_1 P_k, \tag{29}$$

where the parameter $\gamma = \frac{\varepsilon}{k}$ is proportional to the specific dissipation rate ($\gamma = C_\mu \omega$). The turbulent dispersion coefficients are given by $d_k = \frac{\nu_T}{\sigma_k}$ and $d_\varepsilon = \frac{\nu_T}{\sigma_\varepsilon}$. By definition, the source terms in the right-hand side are nonnegative. Furthermore, the parameters ν_T and γ must also be nonnegative for the solution of the convection-reaction-diffusion equations to be well-behaved [3]. In our numerical algorithm, their values are taken from the previous iteration and their positivity is secured as explained below. This linearization technique was proposed by Lew *et al.* [14] who noticed that the positivity of the lagged coefficients is even more important than that of the transported quantities and can be readily enforced without violating the discrete conservation principle.

Applying an implicit FEM-TVD scheme to the above equations, we obtain two nonlinear algebraic systems which can be written in the generic form

$$A(u^{(l+1)})u^{(l+1)} = B(u^{(l)})u^{(l)} + q^{(k)}, \qquad l = 0, 1, 2, \ldots \tag{30}$$

Here k is the index of the outermost loop in which the velocity $\mathbf{u}$ and the source term P_k are updated. The index l refers to the outer iteration for the $k-\varepsilon$ model, while the index m is reserved for inner flux/defect correction loops of the form (22).

The structure of the involved matrices A and B is as follows:

$$A(u) = M_L - \theta \Delta t (K^*(u) + T), \tag{31}$$

$$B(u) = M_L + (1-\theta)\Delta t (K^*(u) + T), \tag{32}$$

where $K^*(u)$ is the LED transport operator incorporating nonlinear antidiffusion and T denotes the standard reaction-diffusion operator which is a symmetric positive-definite matrix with nonnegative off-diagonal entries. It is obvious that the discretized production terms $q^{(k)}$ are also nonnegative. Thus, the positivity of $u^{(l)}$ is inherited by the new iterate $u^{(l+1)} = A^{-1}(Bu^{(l)} + q^{(k)})$ provided that $\theta = 1$ (backward Euler method) or the time step is sufficiently small (satisfies the CFL-like condition for $\theta < 1$). Another important prerequisite is the convergence of nonlinear iterations for the system at hand.

7.2 Positivity of coefficients

The predicted values $k^{(l+1)}$ and $\varepsilon^{(l+1)}$ are used to recompute the parameter $\gamma^{(l+1)}$ for the next outer iteration (if any). The turbulent eddy viscosity $\nu_T^{(k)}$ is updated in the outermost loop. In the turbulent flow regime $\nu_T \gg \nu$ and the laminar viscosity ν can be neglected. Hence, we set $\nu_{\text{eff}} = \nu_T$, where the eddy viscosity ν_T is bounded from below by

ν and from above by the maximum admissible mixing length $l_{\max}$ (e.g. the width of the computational domain). Specifically, we define the limited mixing length l_* as

$$l_* = \begin{cases} \frac{\alpha}{\varepsilon} & \text{if} \quad \varepsilon > \frac{\alpha}{l_{\max}} \\ l_{\max} & \text{otherwise} \end{cases}, \qquad \text{where} \quad \alpha = C_\mu k^{3/2} \tag{33}$$

and use it to update the turbulent eddy viscosity ν_T in the outermost loop:

$$\nu_T = \max\{\nu, l_* \sqrt{k}\} \tag{34}$$

as well as the parameter γ in each outer iteration for the $k-\varepsilon$ model:

$$\gamma = C_\mu \frac{k}{\nu_*}, \qquad \text{where} \quad \nu_* = \max\{\nu, l_* \sqrt{k}\}. \tag{35}$$

A remark is in order that the positivity proof is only valid for the converged solution to (30) while intermediate values of the approximate solution may be negative. Since it is impractical to perform many defect correction steps in each outer iteration, it is worthwhile to substitute $k_* = \max\{0, k\}$ for k in formulae (33)–(35) so as to to prevent taking the square root of a negative number. Upon convergence, this safeguard will not make any difference, since k will be nonnegative from the outset. The above representation of ν_T and γ makes it possible to preclude division by zero and obtain bounded coefficients without making any *ad hoc* assumptions and affecting the actual values of k and ε.

7.3 Initial conditions

Another important issue which is seldom addressed in the CFD literature is the initialization of data for the $k-\varepsilon$ model. As a rule, it is rather difficult to devise a reasonable initial guess for a steady-state simulation or proper initial conditions for a dynamic one. The laminar Navier-Stokes equations remain valid until the flow gains enough momentum for the turbulent effects to become pronounced. Therefore, the $k-\varepsilon$ model should be activated at a certain time $t_* > 0$ after the startup. During the 'laminar' initial phase ($t \le t_*$), a constant effective viscosity ν_0 is prescribed. The values to be assigned to k and ε at $t = t_*$ are uniquely defined by the choice of ν_0 and of the default mixing length $l_0 \in [l_{\min}, l_{\max}]$ where $l_{\min}$ corresponds to the size of the smallest admissible eddies:

$$k_0 = \left(\frac{\nu_0}{l_0}\right)^2, \qquad \varepsilon_0 = C_\mu \frac{k_0^{3/2}}{l_0} \qquad \text{at} \quad t \le t_*. \tag{36}$$

This strategy was adopted as the effective viscosity ν_0 and the mixing length l_0 are easier to estimate (at least for a CFD practitioner) than k_0 and ε_0. In any case, long-term simulation results are typically not very sensitive to the choice of initial data.

7.4 Boundary conditions

At the inlet Γ_{in}, we prescribe all velocity components and the values of k and ε:

$$\mathbf{u} = \mathbf{g}, \qquad k = c_{bc}|\mathbf{u}|^2, \qquad \varepsilon = C_\mu \frac{k^{3/2}}{l_0} \qquad \text{on} \quad \Gamma_{\text{in}}, \tag{37}$$

where $c_{bc} \in [0.001, 0.01]$ is an empirical constant [3] and $|\mathbf{u}| = \sqrt{\mathbf{u} \cdot \mathbf{u}}$ is the Euclidean norm of the velocity. At the outlet Γ_{out}, the normal gradients of all scalar variables are required to vanish, and the 'do-nothing' [19] boundary conditions are prescribed:

$$\mathbf{n} \cdot \mathcal{S}(\mathbf{u}) = \mathbf{0}, \qquad \mathbf{n} \cdot \nabla k = 0, \qquad \mathbf{n} \cdot \nabla \varepsilon = 0 \qquad \text{on} \quad \Gamma_{\text{out}}. \tag{38}$$

Here $\mathcal{S}(\mathbf{u}) = -\left(p + \frac{2}{3}k\right)\mathcal{I} + (\nu + \nu_T)[\nabla \mathbf{u} + (\nabla \mathbf{u})^T]$ denotes the effective stress tensor. The numerical treatment of inflow and outflow boundary conditions does not present any difficulty. In the finite element framework, relations (38) imply that the surface integrals resulting from integration by parts vanish and do not need to be assembled.

At an impervious solid wall Γ_w, the normal component of the velocity must vanish, whereas tangential slip is permitted in turbulent flow simulations. The implementation of the no-penetration (free slip) boundary condition

$$\mathbf{n} \cdot \mathbf{u} = 0 \qquad \text{on} \quad \Gamma_w \tag{39}$$

is nontrivial if the boundary of the computational domain is not aligned with the axes of the Cartesian coordinate system. In this case, condition (39) is imposed on a linear combination of several velocity components whereas their boundary values are unknown. Therefore, standard implementation techniques for Dirichlet boundary conditions based on a modification of the corresponding matrix rows [19] cannot be used.

In order to set the normal velocity component equal to zero, we nullify the off-diagonal entries of the preconditioner $A(\mathbf{u}^{(m)}) = \{a_{ij}^{(m)}\}$ in the defect correction loop (22). This enables us to compute the boundary values of the vector $\mathbf{u}$ explicitly before solving a sequence of linear systems for the velocity components:

$$a_{ij}^{(m)} := 0, \quad \forall j \neq i, \qquad \mathbf{u}_i^* := \mathbf{u}_i^{(m)} + \mathbf{r}_i^{(m)}/a_{ii}^{(m)} \qquad \text{for} \quad \mathbf{x}_i \in \Gamma_w. \tag{40}$$

In the next step, we project the predicted values $\mathbf{u}_i^*$ onto the tangent vector/plane and constrain the corresponding entry of the defect vector $\mathbf{r}_i^{(m)}$ to be zero

$$\mathbf{u}_i^{(m)} := \mathbf{u}_i^* - (\mathbf{n}_i \cdot \mathbf{u}_i^*)\mathbf{n}_i, \qquad \mathbf{r}_i^{(m)} := 0 \qquad \text{for} \quad \mathbf{x}_i \in \Gamma_w. \tag{41}$$

After this manipulation, the corrected values $\mathbf{u}_i^{(m)}$ act as Dirichlet boundary conditions for the solution $\mathbf{u}_i^{(m+1)}$ at the end of the defect correction step. As an alternative to the implementation technique of predictor-corrector type, the projection can be applied to the residual vector rather than to the nodal values of the velocity:

$$a_{ij}^{(m)} := 0, \quad \forall j \neq i, \qquad \mathbf{r}_i^{(m)} := \mathbf{r}_i^{(m)} - (\mathbf{n}_i \cdot \mathbf{r}_i^{(m)})\mathbf{n}_i \qquad \text{for} \quad \mathbf{x}_i \in \Gamma_w. \tag{42}$$

For Cartesian geometries, the algebraic manipulations to be performed affect just the normal velocity component. Note that virtually no extra programming effort is required, which is a significant advantage as compared to another feasible approach based on local coordinate transformations during the finite element matrix assembly [4].

7.5 Wall functions

To complete the problem statement, we still need to prescribe the tangential stress as well as the boundary values of k and ε on Γ_w. Note that the equations of the $k-\varepsilon$ model are invalid in the vicinity of the wall where the Reynolds number is rather low and viscous effects are dominant. In order to avoid the need for resolution of strong velocity gradients, *wall functions* can be derived using the boundary layer theory and applied at an internal boundary Γ_δ located at a distance δ from the solid wall Γ_w [15],[16],[17].

In essence, a boundary layer of width δ is removed from the actual computational domain Ω and the equations are solved in the reduced domain Ω_δ subject to the following empirical boundary conditions:

$$\mathbf{n}\cdot\mathcal{D}(\mathbf{u})\cdot\mathbf{t} = -u_\tau^2\frac{\mathbf{u}}{|\mathbf{u}|}, \qquad k=\frac{u_\tau^2}{\sqrt{C_\mu}}, \qquad \varepsilon=\frac{u_\tau^3}{\kappa\delta} \qquad \text{on} \quad \Gamma_\delta. \tag{43}$$

Here $\mathcal{D}(\mathbf{u}) = (\nu+\nu_T)[\nabla\mathbf{u}+(\nabla\mathbf{u})^T]$ is the viscous part of the stress tensor, the unit vector $\mathbf{t}$ refers to the tangential direction, $\kappa = 0.41$ is the von Kármán constant and u_τ is the *friction velocity* which is assumed to satisfy the nonlinear equation

$$g(u_\tau) = |\mathbf{u}| - u_\tau\left(\frac{1}{\kappa}\log y^+ + 5.5\right) = 0 \tag{44}$$

in the *logarithmic layer*, where the local Reynolds number $y^+ = \frac{u_\tau\delta}{\nu}$ is in the range $20 \le y^+ \le 100$, and be a linear function of y^+ in the *viscous sublayer*, where $y^+ < 20$. Note that $\mathbf{u}$ is the tangential velocity as long as condition (39) is imposed on Γ_δ.

Equation (44) can be solved iteratively, e.g., by Newton's method [15]:

$$u_\tau^{l+1} = u_\tau^l - \frac{g(u_\tau^l)}{g'(u_\tau^l)} = u_\tau^l + \frac{|\mathbf{u}| - u_\tau f(u_\tau^l)}{1/\kappa + f(u_\tau^l)}, \qquad l=0,1,2,\ldots \tag{45}$$

where the auxiliary function f is given by

$$f(u_\tau) = \frac{1}{\kappa}\log y_*^+ + 5.5, \qquad y_*^+ = \max\left\{20, \frac{u_\tau\delta}{\nu}\right\}.$$

The friction velocity is initialized by $u_\tau^0 = \sqrt{\frac{\nu|\mathbf{u}|}{\delta}}$ and no iterations are performed if it turns out that $y^+ = \frac{u_\tau^0\delta}{\nu} < 20$. In other words, $u_\tau = u_\tau^0$ in the viscous sublayer. Moreover, we use $y_*^+ = \max\{20, y^+\}$ in the Newton iteration to guarantee that the approximate solution belongs to the logarithmic layer and remains bounded for $y^+ \to 0$.

The friction velocity u_τ is plugged into (43) to compute the tangential stress, which yields a natural boundary condition for the velocity. Integration by parts in the weak form of the incompressible Navier-Stokes equations gives rise to a surface integral over the internal boundary Γ_δ which contains the prescribed traction:

$$\int_{\Gamma_\delta} [\mathbf{n} \cdot \mathcal{D}(\mathbf{u}) \cdot \mathbf{t}] \cdot \mathbf{v} \, ds = - \int_{\Gamma_\delta} u_\tau^2 \frac{\mathbf{u}}{|\mathbf{u}|} \cdot \mathbf{v} \, ds. \tag{46}$$

The free slip condition (39) overrides the normal stress and Dirichlet boundary conditions for k and ε are imposed in the strong sense. For further details regarding the implementation of wall laws the reader is referred to [15],[16],[17].

7.6 Underrelaxation for outer iterations

Due to the intricate coupling of the governing equations, it is sometimes worthwhile to use a suitable underrelaxation technique in order to prevent the growth of numerical instabilities and secure the convergence of outer iterations. This task can be accomplished by limiting the computed solution increments before applying them to the last iterate:

$$u^{(m+1)} := u^{(m)} + \omega^{(m)}(u^{(m+1)} - u^{(m)}) \qquad \text{where} \quad 0 \le \omega^{(m)} \le 1. \tag{47}$$

The damping factor $\omega^{(m)}$ may be chosen adaptively so as to accelerate convergence and minimize the error in a certain norm [19]. However, fixed values (for example, $\omega = 0.8$) usually suffice for practical purposes. The sort of underrelaxation can be used in all loops (indexed by k, l and m) and applied to selected dependent variables like k, ε or ν_T.

Furthermore, the m-loops lend themselves to the use of an *impicit underrelaxation* strategy which increases the diagonal dominance of the preconditioner [5],[18]:

$$a_{ii}^{(m)} := a_{ii}^{(m)} / \alpha^{(m)}, \qquad \text{where} \quad 0 \le \alpha^{(m)} \le 1. \tag{48}$$

The scaling of the diagonal entries does not affect the converged solution and proves more robust than *explicit underrelaxation* (47). In fact, no underrelaxation whatsoever is needed for moderate time steps which are typically used in dynamic simulations.

7.7 Linear solvers and time step

Finally, let us briefly discuss the choice of the linear solver and of the time discretization. In many cases, explicit schemes are rather inefficient due to severe stability limitations which require taking impractically small time steps. For this reason, we restrict ourselves to the implicit Crank-Nicolson and backward Euler methods which are unconditionally stable and permit large time steps at the expense of solving nonsymmetric linear systems. In our experience, BiCGSTAB and geometric multigrid constitute excellent solvers as long as the parameters are properly tuned and the underlying smoothers/preconditioners are consistent with the size of the time step. If Δt is rather small, standard components like Jacobi, Gauß-Seidel and SOR schemes will suffice. For large time steps, the condition number of the matrix deteriorates and convergence may fail. This can be rectified by resorting to an ILU factorization in conjunction with appropriate renumbering.

8 NUMERICAL EXAMPLES

Solid body rotation. To illustrate the performance of the FEM-TVD algorithm, let us start with a 2D benchmark problem which was proposed by LeVeque [13] to assess the ability of the discretization scheme to cope with steep gradients and reproduce smooth profiles with high precision. To this end, a slotted cylinder, a cone and a hump are exposed to the incompressible velocity field $\mathbf{v} = (0.5 - y, x - 0.5)$ and undergo a counterclockwise rotation about the center of the square domain $\Omega = (0, 1) \times (0, 1)$. Initially, each solid body lies within a circle of radius $r_0 = 0.15$ centered at a point with Cartesian coordinates (x_0, y_0). In the rest of the domain, the numerical solution is initialized by zero.

The shapes of the three bodies can be expressed in terms of the normalized distance function for the respective reference point (x_0, y_0)

$$r(x, y) = \frac{1}{r_0}\sqrt{(x - x_0)^2 + (y - y_0)^2}.$$

The center of the slotted cylinder is located at $(x_0, y_0) = (0.5, 0.75)$ and its geometry in the circular region $r(x, y) \leq 1$ is given by

$$u(x, y, 0) = \begin{cases} 1 & \text{if } |x - x_0| \geq 0.025 \ \vee \ y \geq 0.85, \\ 0 & \text{otherwise.} \end{cases}$$

The corresponding analytical expression for the conical body reads

$$u(x, y, 0) = 1 - r(x, y), \qquad (x_0, y_0) = (0.5, 0.25),$$

whereas the shape and location of the hump at $t = 0$ are as follows

$$u(x, y, 0) = 0.25[1 + \cos(\pi \min\{r(x, y), 1\})], \quad (x_0, y_0) = (0.25, 0.5).$$

After one full revolution ($t = 2\pi$) the exact solution to the pure convection equation (1) coincides with the initial data. The numerical solution produced by the FEM-TVD scheme is displayed in Fig. 2. It was computed on a uniform mesh of 128×128 bilinear elements using the second-order accurate Crank-Nicolson time-stepping with $\Delta t = 10^{-3}$. There are no nonphysical oscillations and the resolution of the three bodies is remarkably crisp. Even the narrow bridge of the cylinder is largely preserved although some erosion of the ridges is observed. The irrecoverable numerical diffusion due to mass lumping is alleviated to some extent by the strongly antidiffusive superbee limiter. At the same time, the excessive antidiffusion entails an artificial steepening of the gradients as well as a gradual flattening of the two peaks. Other TVD limiters are more diffusive so that the lumping error is aggravated and a pronounced smearing of the solution profiles ensues. Many additional examples for scalar convection problems as well as for the compressible Euler equations on both triangular and quadrilateral meshes can be found in [10],[11].

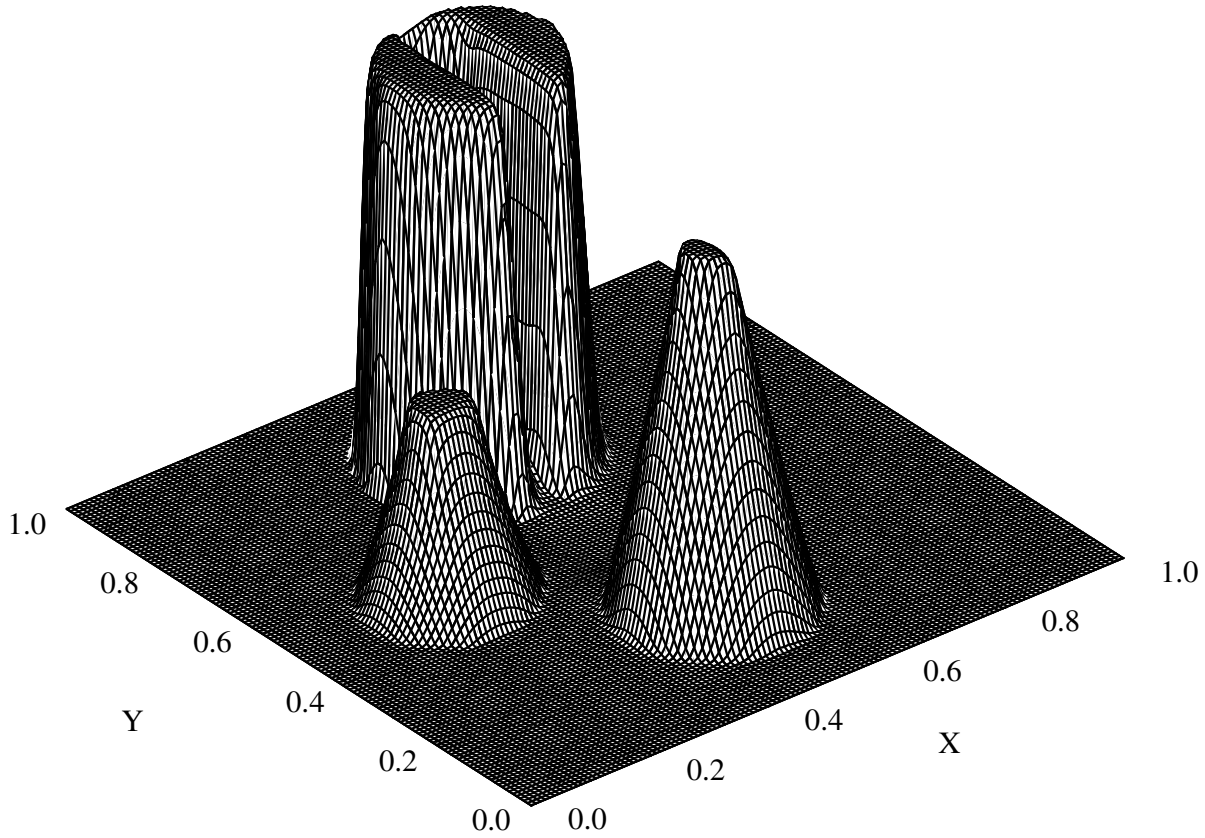

Figure 2: Solid body rotation: FEM-TVD solution at $t = 2\pi$.

Backward facing step. Let us proceed to a three-dimensional test problem which deals with a turbulent flow over a backward facing step at $Re = 44,000$, see [15] for details. Our objective is to validate the implementation of the $k-\varepsilon$ model as described above. In order to satisfy the LBB stability condition, the incompressible Navier-Stokes equations are discretized in space using the nonconforming $\tilde{Q}_1/Q_0$ finite element pair (**discontinuous** rotated trilinear approximation of the velocity and a piecewise-constant pressure) [19]. Standard Q_1 elements are employed for the turbulent kinetic energy and its dissipation rate. All convective terms are handled by the fully implicit FEM-TVD method based on the MC limiter. The velocity-pressure coupling is enforced in the framework of a global MPSC formulation which can be interpreted as a discrete projection method [19].

The stationary distribution of k and ε in the middle cross-section ($z = 0.5$) of the 3D domain is displayed in Fig. 3. The variation of the friction coefficient

$$c_f = \frac{2\tau_w}{\rho_\infty u_\infty^2} = \frac{2u_\tau^2}{u_\infty^2} = \frac{2k}{u_\infty^2}\sqrt{C_\mu}$$

along the bottom wall is presented in Fig. 4 (left). The main recirculation length $L \approx 6.8$

Distribution of k in the cutplane $z = 0.5$

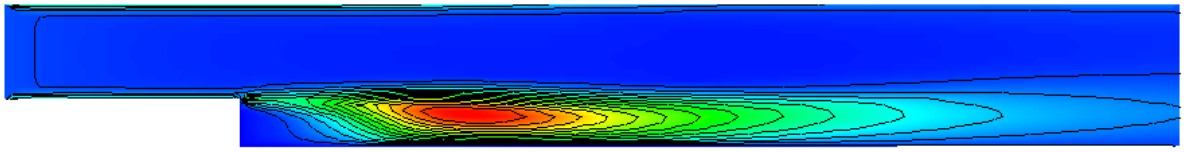

Distribution of ε in the cutplane $z = 0.5$

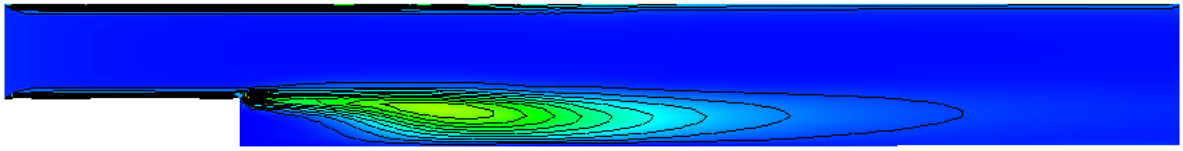

Figure 3: Backward facing step: stationary FEM-TVD solution, $Re = 44,000$.

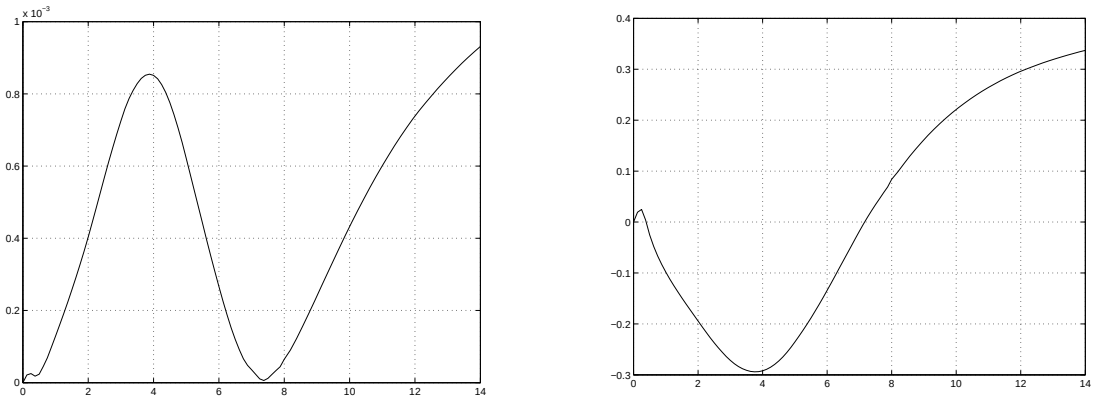

Figure 4: Distribution of c_f (left) and u_x (right) along the bottom wall.

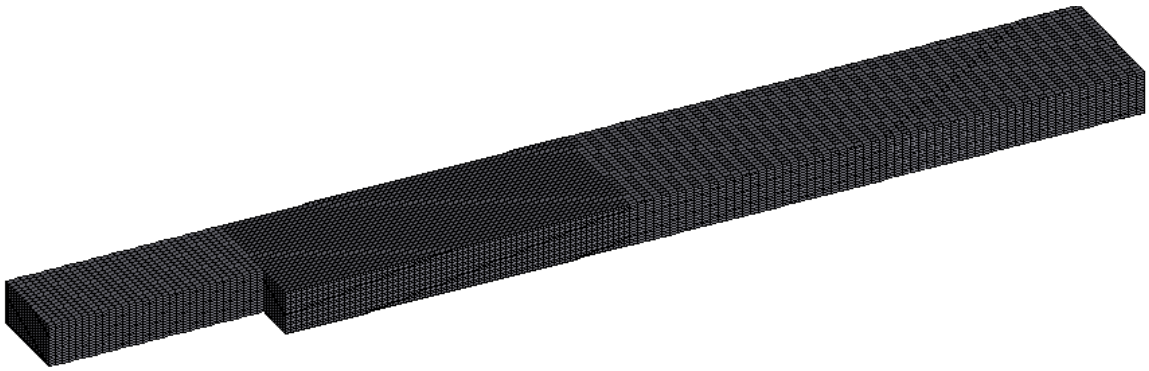

Figure 5: Hexahedral computational mesh for the 3D simulation.

is in a good agreement with the numerical results reported in the literature [15]. Moreover, the horizontal velocity component (see Fig. 4, right) assumes positive values at the bottom of the step, which means that the weak secondary vortex is captured as well. The parameter settings for this three-dimensional simulation were as follows

$$\delta = 0.05, \quad c_{bc} = 0.0025, \quad \nu_0 = 10^{-3}, \quad l_0 = 0.02, \quad l_{\max} = 1.0.$$

Standard wall functions were used on the boundary except for the inlet and outlet. The computational mesh shown in Fig. 5 consisted of 57,344 hexahedra, which corresponds to 178,560 degrees of freedom for each velocity component and 64,073 nodes for k and ε.

9 CONCLUSIONS

A fully multidimensional flux limiter of TVD type was designed so as to render the underlying Galerkin discretization local extremum diminishing and positivity-preserving. This novel approach to the design of high-resolution schemes is very flexible and applicable to a whole range of discretizations (both explicit and implicit time-stepping, finite elements/differences/volumes, triangular and quadrilateral unstructured meshes). In this paper, it was applied to incompressible flow problems in the high Reynolds number regime. The implementation of the $k - \varepsilon$ turbulence model was discussed. Promising simulation results were presented for a three-dimensional benchmark problem. The extension of the proposed algorithm to turbulent bubbly flows in gas-liquid reactors is described in [12].

REFERENCES

[1] J. P. Boris and D. L. Book, Flux-corrected transport. I. SHASTA, A fluid transport algorithm that works. *J. Comput. Phys.* **11** (1973) 38–69.

[2] J.P. Boris, F.F. Grinstein, E.S. Oran und R. J. Kolbe, New insights into Large Eddy Simulation, *Fluid Dynamics Research* **10**, Nr. 4-6, 1992, 199-227.

[3] R. Codina and O. Soto, Finite element implementation of two-equation and algebraic stress turbulence models for steady incompressible flows. *Int. J. Numer. Methods Fluids* **30** (1999) no.3, 309-333.

[4] M. S. Engelman, R. L. Sani and P. M. Gresho, The implementation of normal and/or tangential boundary conditions in finite element codes for incompressible fluid flow. *Int. J. Numer. Meth. Fluids* **2** (1982) 225–238.

[5] J. H. Ferziger and M. Peric, *Computational Methods for Fluid Dynamics*. Springer, 1996.

[6] A. Harten, High resolution schemes for hyperbolic conservation laws. *J. Comput. Phys.* **49** (1983) 357–393.

[7] A. Jameson, Analysis and design of numerical schemes for gas dynamics 1. Artificial diffusion, upwind biasing, limiters and their effect on accuracy and multigrid convergence. *Int. Journal of CFD* **4** (1995) 171-218.

[8] D. Kuzmin, Positive finite element schemes based on the flux-corrected transport procedure. In: K. J. Bathe (ed.), *Computational Fluid and Solid Mechanics*, Elsevier, 887-888 (2001).

[9] D. Kuzmin and S. Turek, Flux correction tools for finite elements. *J. Comput. Phys.* **175** (2002) 525-558.

[10] D. Kuzmin and S. Turek, High-resolution FEM-TVD schemes based on a fully multidimensional flux limiter. Technical report **229**, University of Dortmund, 2003. To appear in *J. Comput. Phys.*

[11] D. Kuzmin and M. Möller, Algebraic Flux Correction. Part I-II. Technical report **249-250**, University of Dortmund, 2004. To appear in: D. Kuzmin, R. Löhner and S. Turek (Eds) *Flux-Corrected Transport: Principles, Algorithms, and Applications*. Springer, Berlin, 2004.

[12] D. Kuzmin and S. Turek, Numerical simulation of turbulent bubbly flows. To appear in Proceedings of the *3rd International Symposium on Two-Phase Flow Modelling and Experimentation*. Pisa, September 22-24, 2004.

[13] R. J. LeVeque, High-resolution conservative algorithms for advection in incompressible flow. *Siam J. Numer. Anal.* **33** (1996) 627–665.

[14] A. J. Lew, G. C. Buscaglia and P. M. Carrica, A note on the numerical treatment of the k-epsilon turbulence model. *Int. J. Comput. Fluid Dyn.* **14** (2001) no.3, 201-209.

[15] G. Medić and B. Mohammadi, NSIKE - an incompressible Navier-Stokes solver for unstructured meshes. *INRIA Research Report* **3644** (1999).

[16] B. Mohammadi, A stable algorithm for the k-epsilon model for compressible flows. *INRIA Research Report* **1355** (1990).

[17] B. Mohammadi and O. Pironneau, *Analysis of the k-epsilon turbulence model*. Wiley, 1994.

[18] S. V. Patankar, *Numerical Heat Transfer and Fluid Flow*. McGraw-Hill, 1980.

[19] S. Turek, *Efficient Solvers for Incompressible Flow Problems: An Algorithmic and Computational Approach*, LNCSE 6, Springer, 1999.

[20] S. T. Zalesak, Fully multidimensional flux-corrected transport algorithms for fluids. *J. Comput. Phys.* **31** (1979) 335–362.